J Bionic Eng 15 (2018) ???–???
DOI: https://doi.org/12345-018-1234-x

Bionic flapping pectoral fin with controllable spatial deformation

Yueri Cai[12*], Lingkun Chen[1], Shusheng Bi[1], Guoyuan Li[2], Houxiang Zhang[2]

1. *Robotics Institute, Beihang University, Beijing, 100191, China*
2. *Department of Ocean Operations and Civil Engineering, Norwegian University of Science and Technology, Aalesund, 6025, Norway*

***Corresponding author:** Yueri Cai
E-mail: caiyueri@buaa.edu.cn

Abstract

This paper presents the biomimetic design of a bionic pectoral fin with fin rays driven by multi-joint mechanism. Inspired by the cownose ray, the bionic pectoral fin is modeled and simplified based on the key structure and movement parameters of the cownose ray's pectoral fin. A novel bionic propulsion fin ray composed of a synchronous belt mechanism and a slider-rocker mechanism is designed and optimized in order to minimize the movement errors between the designed fin rays and the spanwise curves observed from the cownose ray, and thereby reproducing an actively controllable flapping deformation. A bionic flapping pectoral fin prototype is developed accordingly. Observations verify that the bionic pectoral fin flaps consistently with the design rule extracted from the cownose ray. Experiments in a towing tank are set up to test its capability of generating the lift force and the propulsion force. The movement parameters within the usual propulsion capabilities of the bionic pectoral fin are utilized: the flapping frequency of 0.2 Hz-0.6 Hz, the flapping amplitude of 3°-18°, and the phase difference of 10°-60°. The results show that the bionic pectoral fin with actively controllable spatial deformation has expected propulsion performance, which supports that the natural features inspired by the cownose ray play an important role in designing and developing a bionic prototype.

Keywords: cownose ray, bionic pectoral fin, controllable deformation, multiple fin rays, propulsion performance

1 Introduction

Using natural creatures as inspiration provides an effective way to improve the performance of underwater vehicles. Researchers worldwide have sought to use the outstanding characteristics of fish in this manner, including their low-disturbance ability and the high efficiency and high maneuverability [1-3]. The cownose ray offers several advantages as a model for the design of an underwater vehicle. First, the cownose ray's body structure is compact. By exercising precise control over the spatial deformation of its two large flattened pectoral fins, the cownose ray can realize complex swimming modes, such as the pivot turn and the rapid floatation. Second, since its pectoral fin flaps at a very low frequency, varying from 0.4 Hz to 1.2 Hz, its swimming generates minimal hydrodynamic noise [4]. Third, its swimming system that composed of the two pectoral fins, the flexible body and the oscillating tail fins, provides high maneuverability. Fourth, it has a flexible body, which contributes to its ability to move quietly and provides smooth movement deformation and interaction with the surrounding water. Fifth, compared with other elasmobranches that use the undulatory mode, the cownose ray swims with higher velocity via the oscillating mode [4]. Sixth, the cownose ray can manage long-distance migration with high efficiency by combining different swimming modes, such as the normal flapping mode and the gliding movement mode.

The evolutional body structure and the special movement mode of the cownose ray play important roles in realizing its advantages as a model. The fluid optimal outer shape and the body flexibility are beneficial to the low resistance and low noise swim [5, 6], and to the ability to submerge in the surrounding environment [7, 8]. One reason is the passive deformation caused by the interaction between the incoming flow and the flexible fin. Another is the actively controllable deformation, which helps to realize the complex fin shape which adapts to the different swimming conditions. The flexibility of fish fins in nature can be divided into these two classes:

(1) The passive flexibility that is determined by the properties of muscle and cartilage.

(2) The active flexibility that is driven by the muscles and performed by the mechanism composed of

cartilages and muscles.

The complexity of the bionic mechanism can be reduced by applying the flexible mechanism. The spatial movement of the natural pectoral fin can be reproduced by a bionic prototype with a combination of a series of simplified two-dimensional flapping movements. Swimming stability can be improved by applying the flexible mechanism too. It can reduce the force component along the non-driven direction [9]. Research on a rectangular fin with NACA0014 chordwise cross-sections shows that properly arranging the flexibility distribution increases the propulsion efficiency by 36% over the comparable rigid fin [5]. Researches carried out by MIAO JM [10], Katz J [11], and Castelo ME [12] illustrate similar regularity.

The special flapping movements of the cownose ray's pectoral fin is another key biomimetic issue. Different design methods are employed to reproduce the movements, including:

(1) Using a rigid pectoral fin [13], which requires one actuator for each degree of freedom. The driving and transmission system are difficult to design and arrange in the compact space. Further, the spatial deformation and the flexibility of the pectoral fin are omitted.

(2) Applying a soft pectoral fin body driven by a single elastic fin ray [14, 15]. The flexibility distribution of the pectoral fin is pre-designed. Deformation of the pectoral fin cannot be controlled actively when facing different swimming conditions.

(3) Using a thin and flexible bionic pectoral fin driven by multiple straight bars [16, 17], which requires one actuator for each flapping bar. The spanwise deformation and the spatial shape of the pectoral fin are not considered.

(4) Applying a soft bionic pectoral fin [18, 19]. The fin is made completely of soft material, and usually driven by compressed air or novel soft actuators. Its 3D deformation is difficult to control.

The pectoral fin is the main functional part to generate the lift force and the propulsion force. Combining the soft pectoral fin body with the distributed controllable flapping fin rays is a method to mimic

the structures and reproduce the performance of the natural pectoral fins [20].

This paper focuses on the novel design, optimization, and verification of the bionic flapping pectoral fin. The structure and movement characteristics of the cownose ray are abstracted and modeled in Section 2. A novel bionic fin ray system composed of synchronous belt mechanism and slider-rocker mechanism is designed and optimized to reproduce the flapping movements of the cownose ray's pectoral fin, aiming to minimize motion errors. In Section 3, a prototype of the bionic pectoral fin designed is fabricated and assembled. The towing-tank platform is developed according to the requirements of the verification experiments. Movement deformation of the bionic pectoral fin is observed and compared with the cownose ray, as well as the capability of generating the lift force and the propulsion force. In Section 4, we conclude the research work presented, and discuss the future research prospects.

2 Material and methods

2.1 Model of the pectoral fin

Based on the bioresearch results, the typical structural parameters of the cownose ray can be obtained. As shown in Fig. 1, the typical body width S_W of the cownose ray ranges from 0.71 m to 0.92 m, and the body length B_L is about 2/3 times its body width [21]. The typical structure and movement parameters of the cownose ray are shown in Table 1 [22, 23].

Table 1. Typical structure and movement parameters of the cownose ray

Parameters	Typical values
Common width (m)	0.71(female) 0.92(male)
Common weight (kg)	≈ 6
Flapping frequency (Hz)	0.4-1.2 (emergency)
Fin tip flapping amplitude (/fin base length)	≥0.5
Typical number of transmission wave	0.2-0.5
Common velocity (BL/s)	up to 1

Body shape of the cownose ray mainly affects its propulsion performance in two aspects, including (1) reducing hydrodynamic resistance and (2) improving swimming stability. Hydrodynamic resistance is

reduced by its streamlined spatial shape. Series shapes of the cross-sections are illustrated at the right part of Fig. 1. Each cross-section can be simplified to a NACA airfoil [24], with different aspect ratios (the maximum thickness of the airfoil as percent of the chord) increasing from the fin base to the fin tip. The NACA0015 airfoil shape is utilized equally to mimic the cross-sections of the proposed pectoral fin.

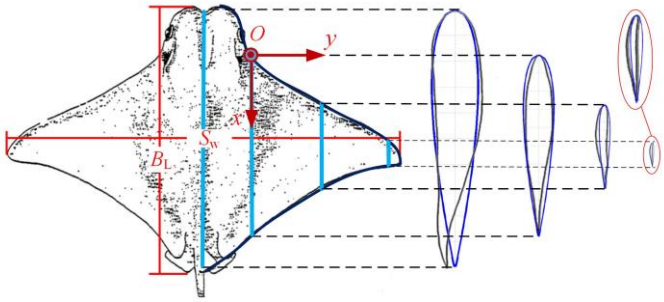

Fig. 1 Structure of the cownose ray and the chordwise shapes of the sample cownose ray on which the design of the pectoral fins is based. The regularized blue shapes on the right illustrate the series of simplified NACA airfoil shapes.

Swimming stability is partly strengthened by the diamond shaped flattened body seen from overhead, as shown in Fig. 1. Each pectoral fin is simplified to an arc-triangle shape. In the analysis, the coordinate system is set as in Fig. 1. The coordinate origin is the intersection point of the leading edge and the fin base line. The fin base line is defined as the chordwise intersecting line between the stationary middle body and the deformable flapping pectoral fin. The *x*-axis points to the tail along with the fin base line. The *y*-axis points to the outside paralleled with the spanwise direction. Curves of the sample cownose ray's leading edge and trailing edge are described separately by

$$\begin{cases} x_l = k_l y + b_l \\ x_t = a_t y^2 + b_t y + c_t \end{cases} \tag{1}$$

where k_l, b_l, a_t, b_t and c_t are constants relating to the different natural cownose ray samples and y is the coordinate values of the points on the edges.

The cownose ray employs the pectoral fin flapping movement, which belongs to the propulsion mode driven by the median and/or pair fins (MPF) [25, 26]. Its complex movement deformation can be divided into

two kinds of sub-motions. One is the flapping motion along the spanwise direction. The other is the wave transmission along the chordwise direction. Quantitative motion analysis is carried out based on the videos of free-swimming cownose rays. A typical series of video frames of a sample cownose ray seen from the back are shown in Fig. 2(a). The spanwise trailing edge curve of the pectoral fin at each time step is abstracted [27], which can be simplified as

$$z(t) = a(t)y^3 \tag{2}$$

where $a(t)$ is a coefficient relating to the time. Further, by analyzing movements of some key points, including the fin tip, the middle point of the leading edge and the middle point of the trailing edge. A general movement rule of the cownose ray can be abstracted. Each point on the edges of the pectoral fin flaps according to

$$A_i = A_{i0}\sin(2\pi\omega_i t + \varphi_{i0}) + A_{i0}^{'} \tag{3}$$

where A_{i0} represents the flapping amplitude of the target point, ω_i represents the flapping frequency, φ_{i0} represents the initial phase, and $A_{i0}^{'}$ represents the flapping offset, that is, whether the upward flapping amplitude is equal to the downward flapping amplitude or not.

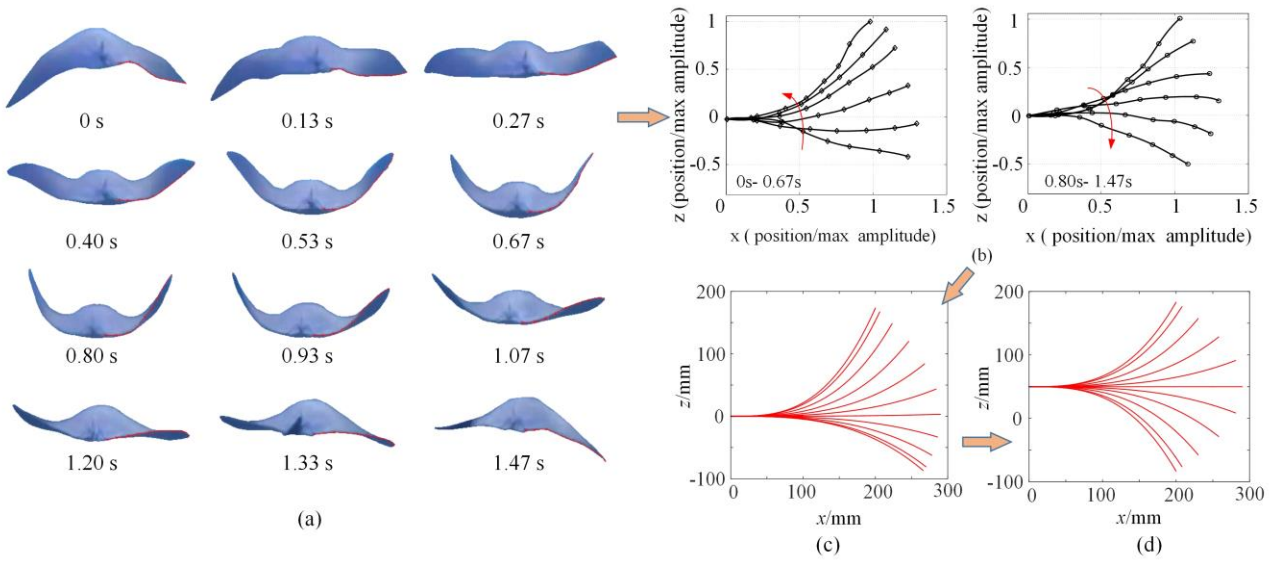

Fig. 2 The spanwise movement model of the cownose ray's pectoral fin. (a) Series snapshots of the cownose ray's pectoral fin, seen from the back view, to illustrate the spanwise deformation during its flapping movement; (b) the trailing edge curves abstracted from the snapshots; (c) the simplified curves with unequal upward and downward amplitude; (d) the optimized curves with equal upward and downward flapping amplitude, which is applied to the bionic design.

The flapping cycle shown in Fig. 2(a) takes 1.47 s, which implies the flapping frequency is 0.68 Hz. As can be seen from Fig. 2(b) and Fig. 2(c), the upward flapping amplitude is about twice that of the downward flapping amplitude, which is defined as the spatial asymmetry of the movement mode of the cownose ray. In this paper, the spatial asymmetry is omitted, in order to make the design and control of the bionic pectoral fin easier.

The sub-motion along the chordwise direction presents as the propulsion wave transmission. Comparing movements of the key points of the sample cownose ray, including the middle point on the leading edge, the fin tip point, and the middle point on the trailing edge, shows that one group of typical flapping frequencies is: 0.38 Hz, 0.40 Hz, and 0.42 Hz. Considering the observation errors, the flapping frequency takes the average value of 0.40 Hz, which is considered to be the flapping frequency of the pectoral fin.

The chordwise movement model can be summarized as [28]

$$\begin{cases} z_1 = 0.07 + 0.28\sin(\int_0^t 2\pi\omega_i dt + 0.283\pi) \\ z_2 = 0.27 + 0.62\sin(\int_0^t 2\pi\omega_i dt + 0.117\pi) \\ z_3 = 0.09 + 0.17\sin(\int_0^t 2\pi\omega_i dt + 0.011\pi) \end{cases} \tag{4}$$

where z_1, z_2, and z_3 represent the normalized positions of the three key points, and ω_i is the flapping frequency of the pectoral fin. Parameters of the chordwise transmission wave can be derived accordingly. The phase differences between the middle point on the leading edge and the fin tip, and between the fin tip and the middle point on the trailing edge are about 30° and 20°, respectively, which means the propulsion wave transmitted along the chordwise direction is approximately 0.3 of a full wave length.

2.2 The bionic pectoral fin design

The mechanical design of the bionic pectoral fin consists of two main parts. One is the driving mechanism that produces the movement rules. The other is realization of the spatial shape and the flexible

feature of the bionic pectoral fin.

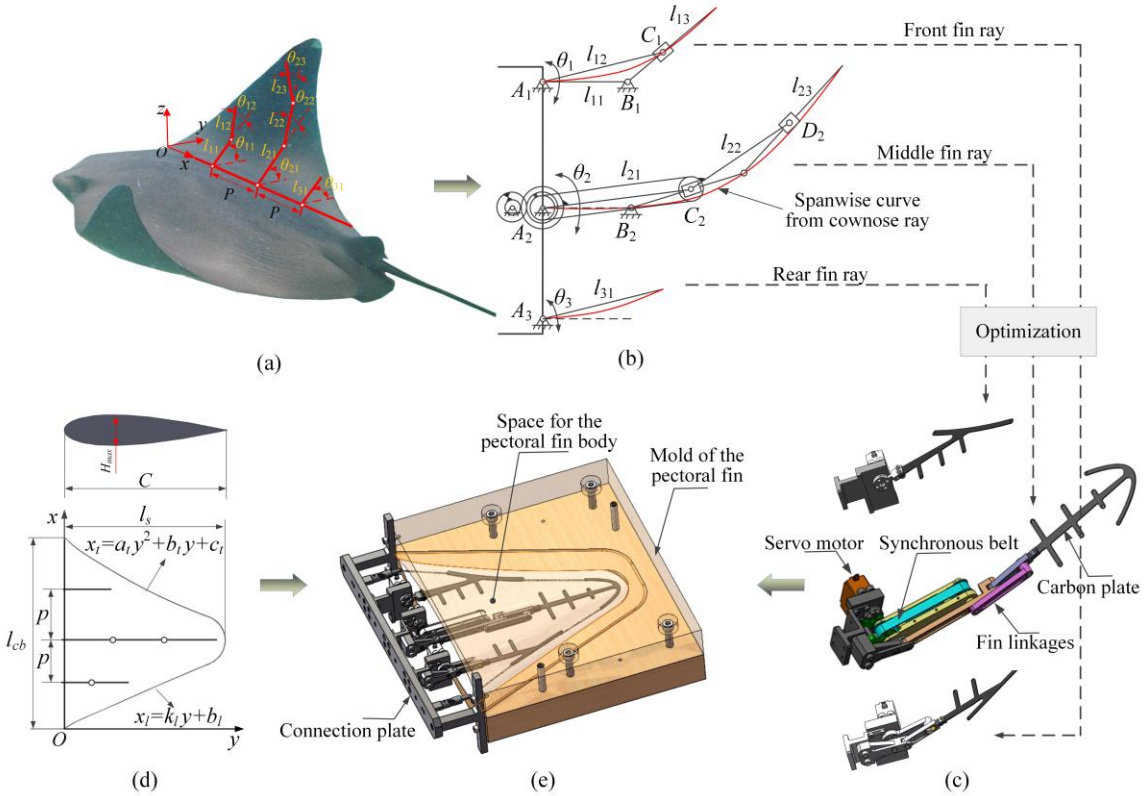

Fig. 3 Design procedure of the bionic pectoral fin. (a) Arrangements of the fin rays; (b) sketch design of the three fin rays; (c) 3D model design of the three fin rays, with the servo motors and the frames; (d) design of the plain shape and the cross-sections of the bionic pectoral fin; (e) design of the mold and accessories.

As shown in Fig. 3(a), the method of applying multiple fin rays is used to drive the bionic pectoral fin. There are three fin rays placed inside the bionic pectoral fin. The front fin ray has two joints, the middle fin ray has three joints, and the rear fin ray has one joint. They are placed at equal intervals along the chordwise direction and connected to the fin base. Therefore, there are five movement control points for each pectoral fin: the intersection point of the leading edge and the fin base, the middle point on the leading edge, the fin tip, the middle point on the trailing edge, and the intersection point of the trailing edge and the fin base. Schematic design of the fin rays is shown in Fig. 3(b). A one-stage slider-rocker mechanism is used for the front fin ray. The synchronous belt and one-stage slider-rocker mechanism is used for the middle fin ray. The rear fin ray is designed with a single joint. Lengths of the linkages and the rotating joint layout are

optimized in order to reproduce the movement of the pectoral fin. Each fin ray is driven by a high-torque servo motor, as shown in Fig. 3(e). Rated torque of the servo motor selected is 35 kg-cm, when the supply voltage is DC 7.4 V.

The plain shape of the bionic pectoral fin shown in Fig. 3(c) is designed based on equation (1). The coefficients of k_l, b_l, a_t, b_t, c_t are 0.5, 0, 0.002, -1, and 360 respectively, which reflect the bioresearch results. The pectoral fin tip curve is fitted by arc to make the pectoral fin edge curve closed and smooth. All the chordwise sections are of NACA0015 airfoil shape, with the length relationship of H_{max}/C=0.15. Fig. 3(d) shows the mold and the prototype assembly. The mold is designed to fit the shape of the cross-sections. The outer edge of the space for the pectoral fin body is 15 mm away from the outer profile of the fin rays. During pouring, the fin rays are fixed at the middle section of the space for the pectoral fin body.

2.3 Optimization of the Fin Rays

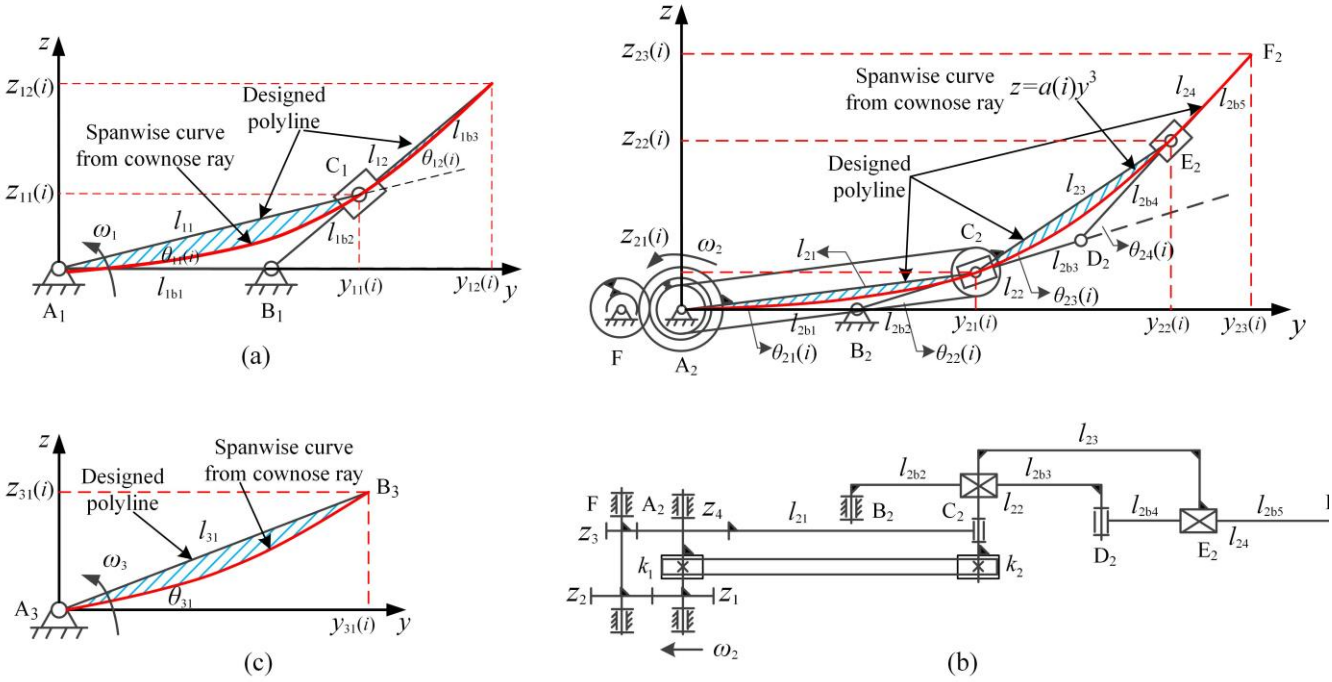

Fig. 4 The optimization schematic of the three fin rays: (a) the front fin ray; (b) the middle fin ray; (c) the rear fin ray.

The front fin ray and the middle fin ray are optimized to fit the spanwise curves extracted from the cownose ray by applying the minimized area difference method. As shown in Fig. 4, the areas marked with

blue slash are the optimization targets, which span from the fin ray curve to the corresponding curve observed from the pectoral fin of the cownose ray at every time step. The optimization is achieved by minimizing the movement errors through properly arranging the linkages and the rotation joints. The rear fin ray uses one flapping linkage, because there is limited space to place it. Its movement error is calculated directly.

In the optimization, the length of the spanwise curves extracted from the cownose ray is supposed to be constant during the flapping movement:

$$\int_0^{Y(i)} \sqrt{1+[3a(i)y^2]^2}\,dy = L \tag{5}$$

where $Y(i)$ is the coordinate value of the spanwise curve at each time step, L is the fixed length of the spanwise curve, and $a(i)$ is a time-related coefficient to keep the spanwise curve constant. The fin ray tip point and the rotation joints are supposed to be on the ideal curve at any moment.

As an example shown in Fig. 4(a) with blue slashes, the objective function is the sum of the area difference $\Delta S(i)$ between the designed polyline and the ideal spanwise curve from the cownose ray over time.

$$Error = \sum_{i=1}^{N} \left|\Delta S(i)\right| \tag{6}$$

where N is the number of the chosen time steps in a whole cycle. N=60 is used here. The absolute values are used to evaluate the fitness performance in the whole cycle. The following discusses optimization of the three fin rays in detail.

The one-stage slider-rocker mechanism is applied to the front fin ray. Fig. 4(a) shows the lengths of the linkages and the angles, which can be calculated as

$$\begin{cases} y_{11}(i) = l_{11}\cos\theta_{11}(i) \\ z_{11}(i) = l_{11}\sin\theta_{11}(i) \\ y_{12}(i) = y_{11}(i) + l_{1b3}\cos[\theta_{11}(i)+\theta_{12}(i)] \\ z_{12}(i) = z_{11}(i) + l_{1b3}\sin[\theta_{11}(i)+\theta_{12}(i)] \end{cases} \tag{7}$$

The optimization constraints are

$$l_{11} + l_{1b3} = 55,\ l_{1b3} \geq l_{11} \geq 0 \tag{8}$$

The relationship between the l_{1b3} and l_{11} is decided according to the characteristics of the cartilages of the cownose ray. That is, from the fin base to the fin tip along the spanwise direction, lengths of the cartilages of cownose ray become longer. Total length of the fin ray, i.e., the sum of l_{11} and l_{1b3}, is determined according to the pectoral fin edge curve and the chordwise position where the front fin ray is placed.

Fig. 4(b) shows the synchronous belt and one-stage slider-rocker mechanism applied to the middle fin ray. The lengths of the linkages and the angles are calculated as

$$\begin{cases} y_{21}(i) = l_{21}\cos\theta_{21}(i) \\ z_{21}(i) = l_{21}\sin\theta_{21}(i) \\ y_{22}(i) = y_{21}(i) + l_{23}\cos[\theta_{23}(i) + \theta_{22}(i)] \\ z_{22}(i) = z_{21}(i) + l_{23}\sin[\theta_{23}(i) + \theta_{22}(i)] \\ y_{23}(i) = y_{22}(i) + l_{2b5}\cos[\theta_{24}(i) + \theta_{22}(i)] \\ z_{23}(i) = z_{22}(i) + l_{2b5}\sin[\theta_{24}(i) + \theta_{22}(i)] \\ l_{2b1} = \dfrac{l_{21}\sin[\theta_{22}(i) - \theta_{21}(i)]}{\sin[\pi - \theta_{22}(i)]} \\ l_{2b2} = \dfrac{l_{21}\sin\theta_{21}(i)}{\sin[\pi - \theta_{22}(i)]} \\ l_{2b4} = \dfrac{l_{23}\sin\theta_{23}(i)}{\sin[\pi - \theta_{24}(i)]} \\ l_{2b2} = \sqrt{l_{21}^2 + l_{2b1}^2 - 2l_{21}l_{2b1}\cos\theta_{21}(i)} \\ l_{22} = l_{2b2} + l_{2b3} \\ l_{24} = l_{2b4} + l_{2b5} \end{cases} \tag{9}$$

$$\begin{cases} \theta_{22}(i) = \arcsin[\dfrac{l_{21}\sin\theta_{21}(i)}{l_{2b2}}] \\ \theta_{23}(i) = k\theta_{21}(i) \\ \theta_{22}(i) = \arcsin[\dfrac{l_{21}\sin\theta_{21}(i)}{\sqrt{l_{21}^2 + l_{2b1}^2 - 2l_{21}l_{2b1}\cos\theta_{21}(i)}}] \\ \theta_{24}(i) = \arcsin[\dfrac{l_{23}\sin\theta_{23}(i)}{\sqrt{l_{23}^2 + l_{2b3}^2 - 2l_{23}l_{2b3}\cos\theta_{23}(i)}}] \end{cases} \tag{10}$$

The optimization constraints are

$$l_{21} + l_{23} + l_{2b5} = 300,\ l_{2b5} \geq l_{23} \geq l_{21} \geq l_{22} \geq 0 \tag{11}$$

The same standard used for the optimization of the front fin ray is applied to decide the relationships among the l_{2b5}, l_{23}, l_{21} and l_{22}, and the flapping amplitude of A=175 mm. The coefficient k is designed as k=1.

Fig. 4(c) shows the rear fin ray using a single joint mechanism. The length of the rear fin ray is decided directly by the spanwise length at its position. The area difference errors in the whole flapping cycle are calculated using the same method expressed in equation (6). One elastic plate will be used for the rear fin ray, which will compensate for the movement errors to certain extent. The calculated movement error is 9.063e+03 mm^2.

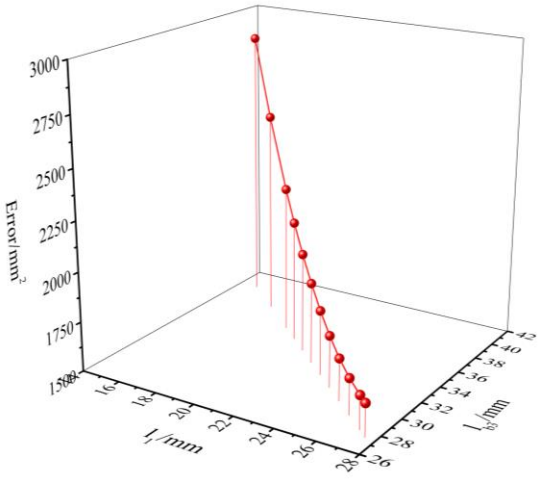

(a)

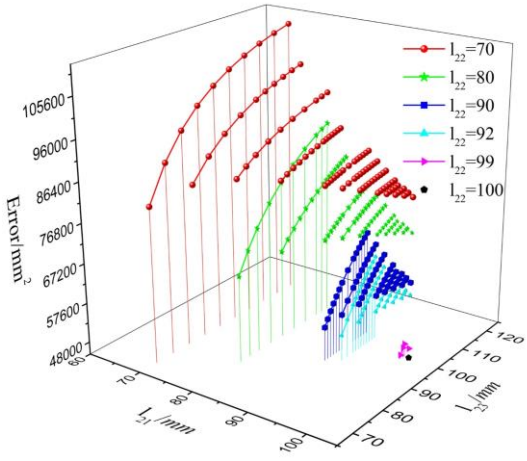

(b)

Fig.5 Movement errors of the front fin ray and the middle fin ray during the whole cycle: (a) optimization results of the front fin ray; (b) optimization results of the middle fin ray.

Each spanwise fin ray of the cownose ray has dozens of short cartilages. The fin ray can flap in large amplitude, according to the sum of each cartilage's small amplitude oscillation. Whereas, limited by the dimension and quality of the actuators and the structural parts, the proposed biomimetic design uses many fewer linkages. Based on the schematic design, the optimization results are shown in Fig. 5. For the front fin ray using two linkages, the movement errors decrease with the length differences between the linkages, as shown in Fig. 5(a). For example, when l_{11}=15 mm, l_{1b3}=40 mm, the total movement error is 2.870+03 mm^2. When l_{11}=27.483 mm, l_{1b3}=27.517 mm, the total movement error is 1.737e+03 mm^2. As shown in

Table 2, the rounded values of l_{11}=27.5 mm, l_{1b3}=27.5 mm are obtained. Accordingly, the length of l_{12} is set at 33.7 mm to ensure the variation of l_{1b3} is at the minimum during the whole flapping cycle. As shown in Fig. 4(a), the base length of the front fin ray is designed as A_1B_1=15 mm based on the optimized dimensions of the linkages.

Table 2. The optimized length and arrangements of the linkages, for bionic pectoral fin prototype of spanwise width of 300 mm.

Fin ray	linkages	Length (mm)	Errors (mm^2)
Front fin ray	l_{11}	27.5	1.737e+03
	l_{12}	33.7	
Middle fin ray	l_{21}	100	4.447e+04
	l_{22}	100	
	l_{23}	100	
Rear fin ray	l_{31}	65	9.063e+03

For the middle fin ray using a synchronous belt and one-stage slider-rocker flapping mechanism, the movement errors between the ideal curves and the designed mechanism change according to a similar rule as the front fin ray. The l_{21}, l_{23}, and l_{2b5} fulfill the condition of equation (11). Thus, when values of any two of them are determined, the third one can be uniquely determined. The optimization error results on the basis of changing l_{22} are shown in Fig. 5(b). As the length difference among the l_{21}, l_{22}, l_{23}, and l_{2b5} becomes smaller, the total movement error in a whole flapping cycle becomes smaller. For example, when l_{21}=65 mm, l_{22}=60 mm, l_{23}=90 mm, and l_{2b5}=145 mm, the movement error can reach 1.146e+05 mm^2. When l_{21}=100 mm, l_{22}=90 mm, l_{23}=90 mm, and l_{2b5}=100 mm, the movement error decreases to 6.185e+04 mm^2. When l_{21}=100 mm, l_{22}=100 mm, l_{23}=100 mm, and l_{2b5}=100 mm, the minimized movement error of 4.447e+04 mm^2 is reached. This is summarized in Table 2. Dimensions of the other linkages of the middle fin ray are determined based on the optimized lengths, including the base length shown in Fig. 4(b) as A_2B_2=15 mm.

3 Results and Discussion

3.1 Development of the bionic pectoral fin

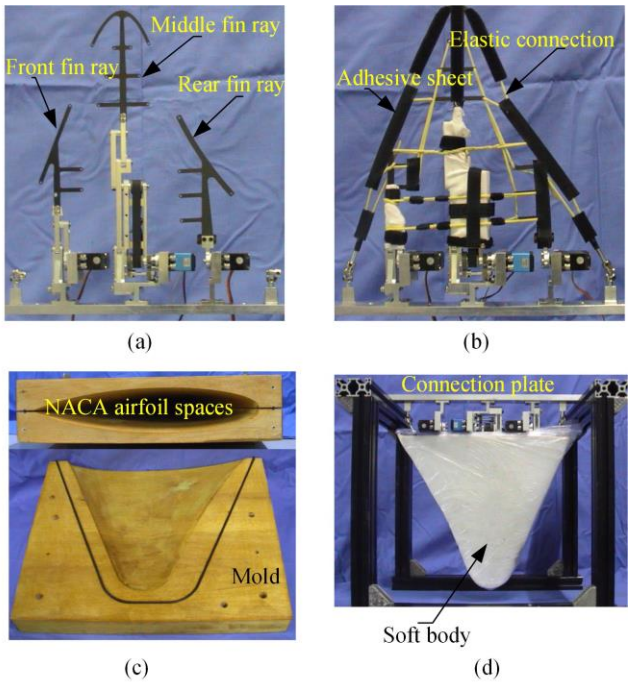

Fig. 6 Development of the bionic pectoral fin prototype: (a) the skeleton of the fin rays with the driving servomotors and the support; (b) the skeleton with the strengthened connecting parts; (c) the mold; (d) the finished bionic pectoral fin prototype with the connection plate.

The bionic pectoral fin prototype is developed according to the optimization results. Fig. 6 shows the fabrication process. As shown in Fig. 6(a), the two linkages of the front fin ray are made of different materials. Parts of the first transmission linkage are made of aluminum, and part of the second linkage are made of carbon plate that is 1.2 mm thick. The shape of the carbon plate is specially designed to meet the flexibility distribution requirements of the leading edge and the connection requirements to the middle fin ray and the soft body. Parts of the first linkage and the second linkage of the middle fin ray are fabricated by aluminum. The third linkage is made of 1.5 mm thick carbon fiber plate. Its special shape is designed to fulfill the outer shape of the pectoral fin. Oscillating movement and torque are transmitted by the synchronous belt system to minimize the dimension of the mechanism in thickness direction.

Some adhesive sheets are added on several parts of the inside skeleton of the pectoral fin, as shown in Fig. 6(b). The soft rubber cannot stick firmly with the aluminum parts or the carbon fiber plates. Without

the adhesive sheet, the inside skeleton and the outer soft body will disconnect during the flapping movements. The elastic connection tubes are fixed along both the spanwise direction and the chordwise direction. They are used to fill the movement gaps between the fin rays, which makes the flapping movements of the bionic pectoral fin smoother. They also help the outer soft body connect with the inside skeleton more firmly. The mold shown in Fig. 6(c) is made of wood with CNC fabrication. Its dimensions are fabricated based on the biomimetic analysis results shown in Fig. 1 and Fig. 3. Considering the pouring process and demolding process, two sub-molds are used to make the bionic pectoral fin prototype easier to remove. Along the profile of the space for the bionic pectoral fin, a sealing groove is designed to avoid leaking of the liquid silicone rubber. Two dowel pins are used to fix the relative position of the two sub-molds. The screw holes are used for fixing the sub-molds and demolding.

Fig. 6(d) shows the finished bionic pectoral fin prototype with a soft outer body. The prototype has the maximum spanwise length of 300 mm and the maximum chordwise length of 360 mm. The soft outer body is made of two-component room temperature silicone rubber. Hardness of the silicone rubber after curing is 20 HA. Its elasticity is three times as large as that of its original dimension. The natural frequency of the bionic pectoral fin's soft body is 4.39 Hz, which is out of the range of the flapping frequency applied to the bionic pectoral fin and has little influence on its flapping stability.

Table 3. Design parameters of the bionic pectoral fin.

Variables	Symbol	Unit	Range of values
Oscillatory amplitude	θ_{max}	degree	0-20
Oscillatory frequency	f	Hz	0-0.6
Phase difference	φ	degree	0-60

The bionic pectoral fin prototype developed combines the active control ability of the inside driving skeleton and the soft outer body. Both the spanwise deformation and the chordwise driving wave transmission can be controlled. Basic movement parameters of the bionic pectoral fin are summarized in Table 3, which reproduce the movement of the cownose ray's pectoral fin to an extent.

3.2 The experimental settings

The towing tank experimental platform is built to observe the movement deformation and propulsion performance of the bionic pectoral fin. It is composed of a control PC, the towing system, the force sensors, the data acquisition device, the bionic pectoral fin, and the driving boards. The main parameters of the sensors and other devices of the towing platform are summarized in Table 4.

Table 4. Parameters of the sensors and the experimental platform

Parameters	Values
Towing speed	0-0.5 m/s
Number of force sensor	2
Force range of the sensor	0-20 N
Measuring accuracy	0.03%F·S
Output signals	4-20 mA or +/-10V

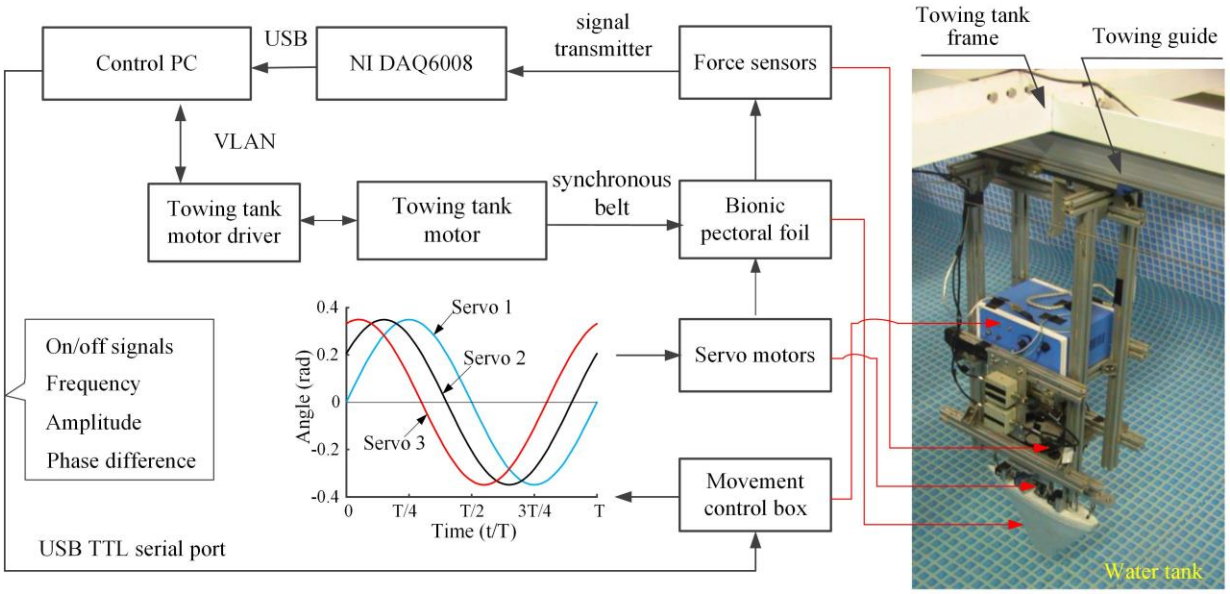

Fig. 7 The experimental settings and the control strategy for the propulsion force and lifting force tests: the left side shows the sensor data flow and the control strategy; the right side shows the towing platform.

A control box of the bionic pectoral fin is developed and fixed on the towing platform. The STM32F103 device is used as its core chip. The sinusoidal control strategy observed from the nature pectoral fin is integrated in the control box, and applied to the servo motors of the front fin ray, the middle fin ray, and the rear fin ray. The sine waves with controllable phase difference are shown in Fig. 7. They

are determined based on the results observed from the cownose ray and the movement ability of the bionic pectoral fin prototype.

Two S-shape HSTL-BLSM-20N force sensors are used to measure the propulsion force and lift force generated by the bionic pectoral fin prototype. The force sensors have been calibrated by suspension of standard weights. The propulsion force and lift force measured will be corrected by the calibration results in the experiments.

3.3 Observation on the spatial deformation

Observation experiments are carried out to verify the designed movement deformation. Eighteen markers are set on the leading edge and on the trailing edge of the bionic pectoral fin. An underwater camera is placed at the fixed distance from the bionic pectoral fin. Flapping movements of the bionic pectoral fin are recorded by the camera with rates of 30 frames per second. The spanwise flapping deformation and the chordwise deformation are extracted from the videos accordingly.

Series snapshots of the spanwise flapping movements seen from behind are shown in Fig. 8(a). The control parameters utilized are θ_{max}=20°, f=0.6 Hz, $\Delta\varphi$=30°. The observations are carried out in still water, and the towing speed is v=0 m/s. Obvious spanwise bending deformation during the flapping movement is obtained from the snapshots. Deformation of both the leading edge and the trailing edge are smooth along the spanwise direction.

Corresponding spanwise curves are extracted from the snapshots by a processing software we developed, as shown in Fig. 8(b). The curves are consistent with the rule extracted from the natural cownose ray in that they approximate the series cubic curves. Compared with the extracted curves, the curvature of the spanwise curves of the bionic pectoral fin is larger. The flapping amplitude of the fin tip is as large as 112 mm, which is less than the designed middle fin ray's achievable amplitude. It is caused mainly by the movement resistance generated by the soft body and the passive deformation of the elastic tip linkages of the fin ray. For example, when the pectoral fin bends upward, the top half soft body is compressed, and the

elastic reaction force will push the bionic pectoral fin to deform downward. Furthermore, the passive deformation of the fin rays' tip linkages and the outer part of the soft body contribute to the performance too. In general, the spanwise bending trend is obtained as designed, which basically verifies the design method.

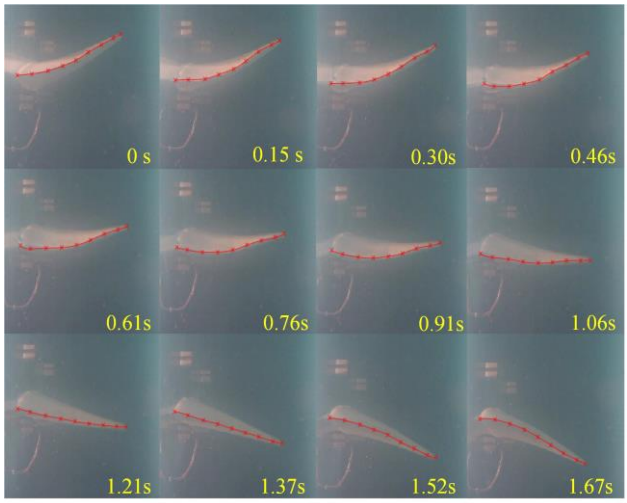

(a)

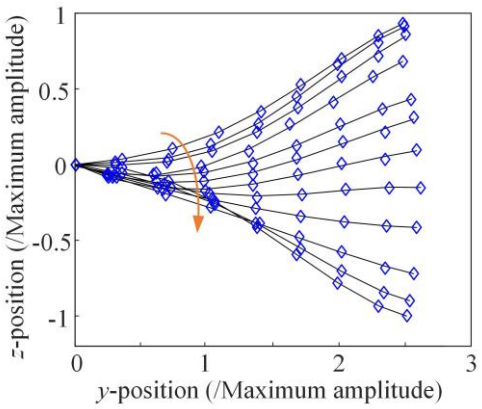

(b)

Fig. 8 The spanwise movement deformation of the bionic pectoral fin. (a) Series snapshots of the bionic pectoral fin in a full cycle flapping; (b) the extracted trailing edge curves.

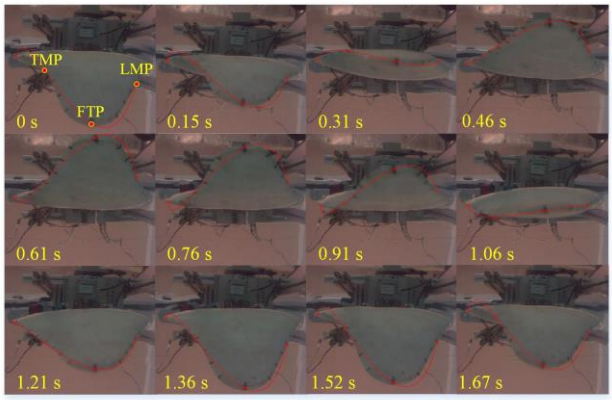

(a)

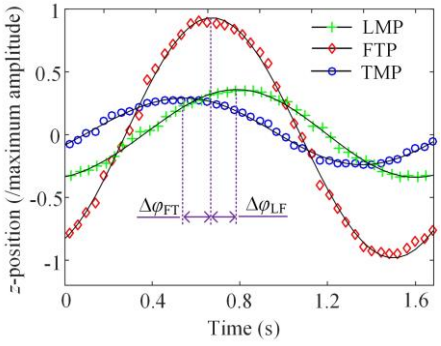

(b)

Fig. 9 The chordwise movement deformation of the bionic pectoral fin. (a) series snapshots of the bionic pectoral fin in a full flapping cycle; (b) the extracted chordwise curves that show the driving wave transmission along chordwise direction; LMP represents the middle point on the leading edge, FTP represents the fin tip point, and TMP represents the middle point on the trailing edge.

Results of observing the chordwise flapping deformation are shown in Fig. 9. The same experimental settings that were applied to observe the spanwise deformation are employed. Fig. 9(a) illustrates the obvious chordwise driving wave transmission. Movements of the markers are in accordance with the sinusoidal rule as designed. Series curves of the leading edge and the trailing edge in a full flapping cycle are extracted and shown in Fig. 9(b). As set in advance, the movement phase of the leading edge leads ahead to the fin tip. The phase difference between the fin tip and the trailing edge performs with the same regularity. It can be observed that the phase difference between the middle point on the leading edge and the fin tip is $\Delta\varphi_{LF}$=0.11 s, and the phase difference between the fin tip and the middle point on the trailing edge is $\Delta\varphi_{FT}$=0.13 s. The two phase differences reach the phase difference 30° applied between the adjacent

two fin rays, i.e., 0.14 s. Then, the number of the average driving wave transmitted along the chordwise direction on the bionic pectoral fin is 0.29 times of a full wave length, which is within the value range observed from the cownose ray. The phase lags performed are smaller than designed. Reasons for the outcome include (I) the drag resistance comes from the soft body made by silicone rubber and (II) the deformation resistance from the elastic connection tube connected among the fin rays.

3.4 Propulsion force and lift force performance

A series of experiments by the towing tank platform are carried out to test influences of the controllable parameters on the lift force and propulsion force. As discussed in Section 2, the controllable parameters include the flapping amplitude of the first linkage of each fin ray θ_{max}, the flapping frequency f, the phase differences between adjacent fin rays of the bionic pectoral fin $\Delta\varphi$, and the towing speed applied to the towing platform v.

The influences of the flapping amplitude on the propulsion forces and the lift forces are shown in Fig. 10(a). The amplitude is controlled to vary from 3° to 18°, which is applied to the first linkages of the three fin rays. The amplitudes of the tips of the fin rays, as well as the corresponding position on the pectoral fin, are amplified by the synchronous belt and slider-rocker mechanism. Corresponding to the selected angle amplitudes, i.e., 3°, 6°, 9°, 12°, 15°, and 18°, the amplitudes of the middle fin ray are: 68.4 mm, 126.1 mm, 168.8 mm, 197.6 mm, 215.4 mm, and 225.6 mm theoretically, which represent the flapping amplitudes of the bionic pectoral fin. Two groups of controlling parameters are selected, including v=0.15 m/s, f=0.4 Hz, $\Delta\varphi$=25° and v=0.3m/s, f=0.3 Hz, $\Delta\varphi$=20°. Within the testing range, the lift force increases with the amplitude becoming larger. The propulsion force conforms to a similar rule. It can be taken as a component of the lift force. When the amplitude is 3° the propulsion forces are negative, which means that the propulsion force under this condition cannot conquer the drag force generated by the bionic pectoral fin under towing. The trends of the lift forces and the propulsion forces illustrate that the bionic fish propelled

by the proposed bionic pectoral fin can be speeded up by simply increasing the flapping amplitudes within this range of flapping amplitudes.

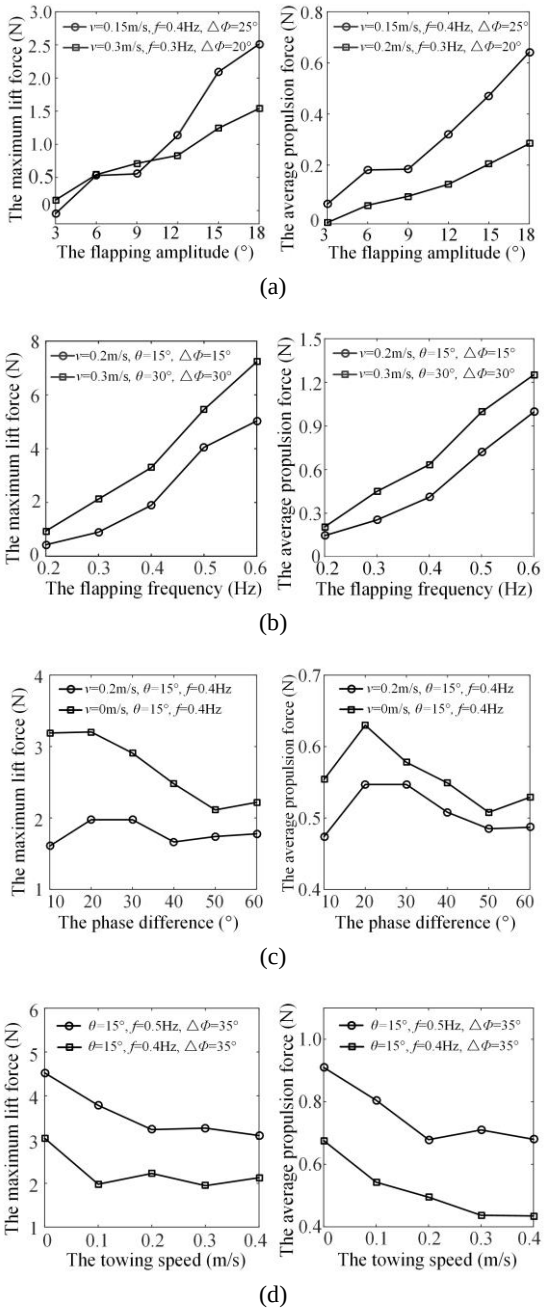

Fig. 10 Influence of the controllable movement parameters on the production ability of the lift force and the propulsion force. (a) the flapping amplitude; (b) the flapping frequency; (c) the phase difference; (d) the towing speed.

The influence of the flapping frequencies on producing the lift force and propulsion are shown in Fig. 10(b). The fin rays are controlled to flap with the frequencies that vary from 0.2 Hz to 0.6 Hz. They can

make the bionic pectoral fin flap with the same frequency uniformly. Two groups of controlling parameters are used, as v=0.2 m/s, θ=15°, $\Delta\varphi$=15° and v=0.3m/s, θ=30°, $\Delta\varphi$=30°. Positive propulsion force can be produced with the low flapping frequency of 0.2 Hz, with both the two groups of parameters. This performance verifies the ability of the cownose ray's low-frequency swimming. Within the testing range of the flapping frequency, the lift force increases obviously with the frequency increasing. The propulsion force illustrates the same trend.

Another controllable parameter considered is the phase difference between the two adjacent fin rays. The phase difference changing ability of the bionic pectoral ranges from 0° to 60°, which equals to 0 to 0.67 times a full length of waves transmitting on the bionic pectoral fin. As can be observed from Fig. 10(c), the lift force and the propulsion force both perform according to the rule that the values increase from 10°, reach the maximum value at around 20°, and then decrease when the phase difference increases. For the designed bionic pectoral fin, the maximum values of the lift force and the propulsion force are obtained at 20°. The equivalent transmission wave number is 0.22. The wave number is less than the optimized wave number observed from the cownose ray, which is mainly caused by the simplification of the bionic mechanism.

The towing movement of the experimental platform mimics the swimming condition of the bionic fish. The towing speeds from 0 m/s to 0.4 m/s are applied with two groups of controllable movement parameters, i.e., θ=15°, f=0.5 Hz, $\Delta\varphi$=35° and θ=15°, f=0.5 Hz, $\Delta\varphi$=35°. Values of the lift force become smaller when the towing speed increases, as shown in Fig. 10(d). The propulsion forces that represent the differences between the forward driving forces produced by the bionic pectoral fin and the drag forces show the same changes. The maximum values are obtained when the towing speed is 0 m/s. For a stable constant forward swimming, the propulsion force is equal to the drag force. Therefore, the absolute forward propulsion force will be near zero. The downward trend indicates that there will be a maximum swimming speed that the

bionic pectoral fin can support.

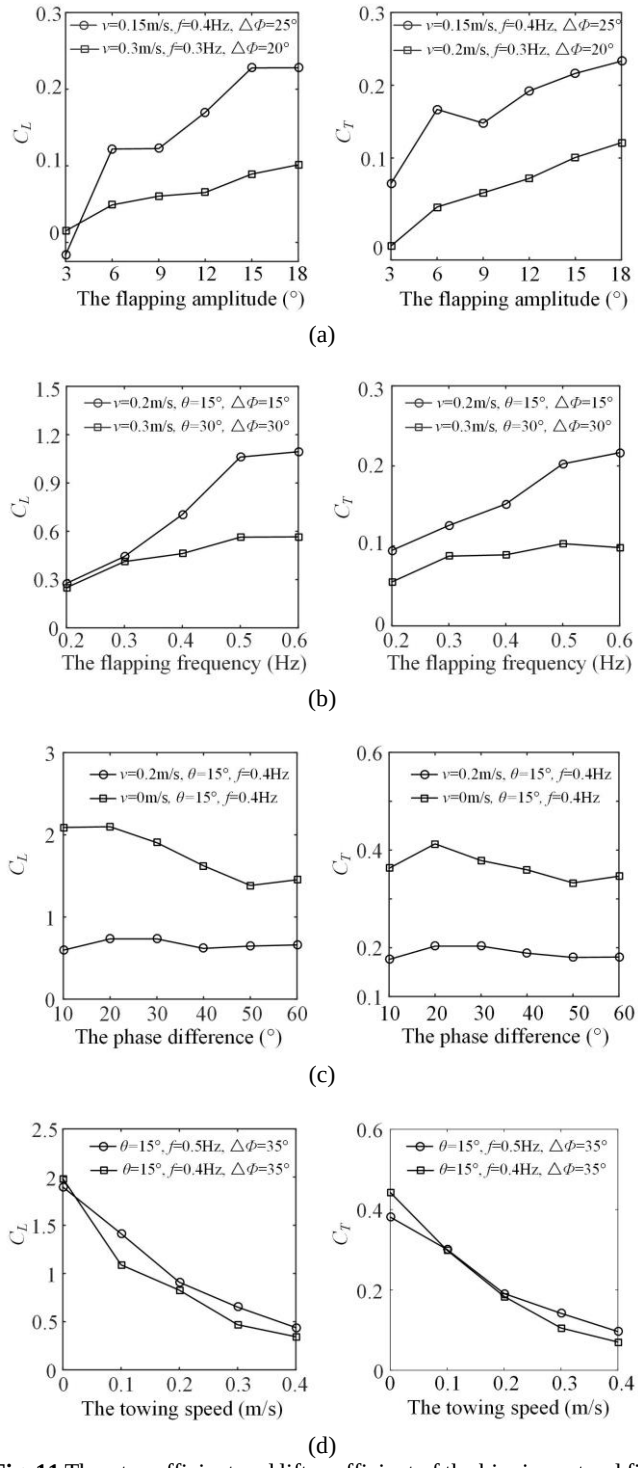

Fig. 11 Thrust coefficient and lift coefficient of the bionic pectoral fin under different movement parameters. (a) the flapping amplitude; (b) the flapping frequency; (c) the phase difference; (d) the towing speed.

The average propulsion force and the maximum lift force are non-dimensionlized by calculating the thrust coefficient C_T and the lift coefficient C_L, under the same movement parameters as used in Fig. 11. The resultant velocity magnitude seen from the fin combining the towing speed and the average flapping velocities of the pectoral fin tip is used in the calculation [29-31].

Within the testing range, the thrust coefficient C_T become bigger as the flapping amplitude increases, as shown in Fig. 11(a). The lift coefficient performs a similar trend. The maximum C_T and the maximum C_L are both obtained when the flapping amplitude is 18°, with values of 0.23 and 0.91, when the movement parameter are v=0.15m/s, f=0.4Hz, $\Delta\varphi$=25°. The flapping frequency affects the thrust coefficient and the lift coefficient in a similar way, as shown in Fig. 11(b). Fig. 11(c) shows that C_T and C_L reach the maximum value at around 20°, and then decrease when the phase difference increases. The changing regularity is the same as the propulsion force and the lift force. Values of C_T and C_L become smaller when the towing speed increases, as shown in Fig. 11(d). The bionic pectoral fin presented performs higher capability of generating propulsion force compared with the soft pectoral fin driven by the actively controlled shape memory alloy and other smart materials [14, 18], for its spatial curvatures and the driving parameters can be actively controlled by the driving fin rays with higher precision. Whereas, compared with the plate-shaped pectoral fin actuated by single or multiple passively deforming fin rays [16, 29], the pectoral fin presented produces lower propulsion forces under the similar motion parameters, due to that the pouring soft pectoral fin body partly restricts the chordwise driving wave transmission and further reduces the thrust force component.

4 Conclusion

This paper proposed a novel design method of bionic pectoral fin following the characteristics of the pectoral fin of the cownose ray. Structural features of the cownose ray's pectoral fin are extracted from the biological literatures, including the body shape, the chordwise cross-sections, and the cartilages'

characteristics. These structural features are utilized to direct the design of the mold, the selection of the silicone rubber for the soft body, the outer shape of the carbon fiber plate that acts as the tip linkage of each fin ray, and the chordwise connecting parts. Movement characteristics of the pectoral fin of the cownose ray are observed, modeled, and utilized to guide the design and optimization of the driving fin rays and the control strategy applied to the bionic pectoral fin prototype. The bionic fin ray mechanism has been optimized by applying the minimized area difference method to make it flap following the simplified movement rules abstracted from the natural cownose ray. For the driving fin ray presented, when the lengths of the three linkages are equal, the minimized movement error in a full flapping cycle of 4.447e+04 mm^2 can be obtained. It means that the bionic pectoral driven by the fin ray in these dimensions can perform high standard bionic flapping movements. The movement deformation performance, as well as capability of generating the lift force and propulsion force of the bionic pectoral fin are verified by the observations and the force testing experiments by the towing tank platform. The influence of the controllable movement parameters on the production of the lift force and the propulsion force under some typical conditions are obtained and analyzed. Results show that the bionic pectoral fin prototype reproduces the flapping movements of the natural pectoral fin to a great extent. The prototype can realize self-propelled function.

Acknowledgement

The work presented in this paper is supported by the Beijing Municipal Natural Science Foundation (No.3182019), the Fundamental Research Funds for the Central Universities (No.YMF-19-BJ-J-345) and the China Scholarship Council (No.201706025027).

Reference

[1] Zhang S W, Qian Y, Liao P, Qin F H, Yang J M. Design and control of an agile robotic fish with integrative biomimetic mechanisms. *IEEE/ASME Transactions on Mechatronics*, 2016, **21**(4), 1846-1857.

[2] Yu J Z, Chen S F, Wu Z X, Chen X Y, Wang M. Energy analysis of a CPG-controlled miniature robotic fish. *Journal of Bionic Engineering*, 2018, **15**(2), 260-269.

[3] Cai Y R, Bi S S, Zheng L C. Design and experiments of a robotic fish imitating cow-nosed ray. *Journal of Bionic Engineering*, 2010, **7**(2), 120-126.

[4] Rosenberger L J. Pectoral fin locomotion in batoid fishes: undulation versus oscillation. *Journal of Experimental Biology*, 2001, **204**(2), 379-394.

[5] Prempraneerach P, Hover F S, Triantafyllou M S. The effect of chordwise flexibility on the thrust and efficiency of a flapping foil. *Proc. 13th Int. Symp. on Unmanned Untethered Submersible Technology: special session on bioengineering research related to autonomous underwater vehicles*, New Hampshire, USA, 2003, 152-170.

[6] Webb P W. Hydrodynamics and energetics of fish propulsion. *Bulletin of the fisheries research board of Canada*, 1975, **190**: 1-159.

[7] Khalid M S U, Jiang X P, Akhtar I, Wu B X. Quantification of flow noise produced by an oscillating foil. *arXiv*, 2018, preprint arXiv:1806.01535.

[8] Zhou K, Liu J K, Chen W S. Study on the hydrodynamic performance of typical underwater bionic foils with spanwise flexibility. *Applied Sciences*, 2017, **7**(11), 1120.

[9] Tang J, Viieru D, Shyy W. A study of aerodynamics of low Reynolds number flexible airfoils. *37th AIAA Fluid Dynamics Conference and Exhibit*, Miami, USA, 2007, p.4212.

[10] Miao J M, Ho M H. Effect of flexure on aerodynamic propulsive efficiency of flapping flexible airfoil. *Journal of Fluids and Structures*, 2006, **22**(3), 401-419

[11] Katz J, Weihs D. Hydrodynamic propulsion by large amplitude oscillation of an airfoil with chordwise flexibility. *Journal of Fluid Mechanics*, 1978, **88**(3), 485-497.

[12] Castelo M E. *Propulsive performance of flexible-chord foils. Doctoral dissertation*. Massachusetts, USA: Department of Ocean Engineering, MIT, 2002.

[13] Kato N. Control performance in the horizontal plane of a fish robot with mechanical pectoral fins. *IEEE journal of oceanic engineering*, 2000, **25**(1), 121-129.

[14] Wang Z L, Wang Y W, Li J, Hang G R. A micro biomimetic manta ray robot fish actuated by SMA. *IEEE International Conference on Robotics and Biomimetics*, Guilin, China, 2009, 1809-1813.

[15] Chew C M, Lim Q Y, Yeo K S. Development of propulsion mechanism for robot manta ray. *IEEE International Conference on Robotics and Biomimetics*, Zhuhai, China, 2015, 1918-1923.

[16] Yang S B, Qiu J, Han X Y. Kinematics modeling and experiments of pectoral oscillation propulsion robotic fish. *Journal of Bionic engineering*, 2009, **6**(2), 174-179.

[17] Zhou C L, Low K H. Better Endurance and Load cap acity: An improved design of manta ray robot (RoMan-II). *Journal of Bionic Engineering*, 2010, **7**(4), 137-144.

[18] Kim H S, Lee J Y, Chu W S, Ahn S H. Design and fabrication of soft morphing ray propulsor: undulator and oscillator. *Soft Robotics*, 2017, **4**(1), 49-60.

[19] Fish F E, Schreiber C M, Moored K W, Liu G, Dong H B, Bart-Smith H. Hydrodynamic performance of aquatic flapping: efficiency of underwater flight in the manta. *Aerospace*, 2016, **3**(3), 20.

[20] Zhang S W, Liu B, Wang L, Yan Q, Low K H, Yang J. Design and implementation of a light weight bioinspired pectoral fin driven by SMA. IEEE/ASME Transactions on Mechatronics, 2014, 19(6),

1773-1785.

[21]Li G Y, Deng Y X, Osen O L, Bi S S, Zhang H X. A bio-inspired swimming robot for marine aquaculture applications: From concept-design to simulation. *OCEANS*, Shanghai, China, 2016, 1-7.

[22]Heine C E. *Mechanics of flapping fin locomotion in the cownose ray, Rhinoptera bonasus (Elasmobranchii: Myliobatidae)*. Duke University, Durham, America, 1993.

[23]Fish F E, Kolpas A, Crossett A, Dudas M A, Moored K W, Bart-Smith H. Kinematics of swimming of the manta ray: three-dimensional analysis of open water maneuverability. *Journal of Experimental Biology*, 2018, **221**(6), jeb-166041.

[24]Abbott I H, Von Doenhoff A E. *Theory of wing sections, including a summary of airfoil data*. Courier Corporation, North Chelmsford, America, 1959.

[25]Blake R W. Fish functional design and swimming performance. *Journal of fish biology*, 2004, **65**(5), 1193-1222.

[26]Lauder G V. Fish locomotion: recent advances and new directions. *Annual review of marine science*, 2015, **7**, 521-545.

[27]Zheng L C, Bi S S, Cai Y R, Niu C M. Design and optimization of a robotic fish mimicking cow-nosed ray. *IEEE International Conference on Robotics and Biomimetics*, Tianjin, China, 2010, 1075-1080.

[28]Cao Y, Bi S S, Cai Y R, Wang Y L. Applying central pattern generators to control the robofish with oscillating pectoral fins. *Industrial Robot: An International Journal*, 2015, **42**(5): 392-405.

[29]Geder J D, Ramamurti R, Pruessner M. Thrust magnitude and efficiency studies for multiple robotic flapping fins. *OCEANS MTS/IEEE*, Washington, USA, 2015, 1-7.

[30]Chew C M, Arastehfar S, Gunawan G, Yeo K S. Study of sweep angle effect on thrust generation of oscillatory pectoral fins. *IEEE/RSJ International Conference on Intelligent Robots and Systems (IROS)*, Vancouver BC, Canada, 2017, 6271-6276.

[31]Kikuchi K, Uehara Y, Kubota Y, Mochizuki O. Morphological considerations of fish fin shape on thrust generation. *Journal of Applied Fluid Mechanics*, 2014, **7**(4), 625-632.